

The Century Survey: A Deeper Slice of the Universe ^{1,2}

Margaret J. Geller, Michael J. Kurtz,
Harvard-Smithsonian Center for Astrophysics, Cambridge, MA 02138

Gary Wegner, John R. Thorstensen,
Department of Physics and Astronomy, Dartmouth College, Hanover, NH 03755-3528

Daniel G. Fabricant,
Harvard-Smithsonian Center for Astrophysics, Cambridge., MA 02138

Ronald O. Marzke,³
Dominion Astrophysical Observatory, Victoria BC V8X 4M6 Canada

John P. Huchra, Rudolph E. Schild, and Emilio E. Falco
Harvard-Smithsonian Center for Astrophysics, Cambridge, MA 02138

ABSTRACT

The ‘‘Century Survey’’ (CS hereafter) is a complete redshift survey of a 1°-wide strip. It covers 0.03 steradians to a limiting $m_R = 16.13$. The survey is 98.4% complete and contains 1762 galaxies. Large-scale features in the survey are qualitatively similar to those in other surveys: there are large voids surrounded or nearly surrounded by thin dense regions which are sections of structures like (and including) the Great Wall.

The survey crosses the classical Corona Borealis supercluster. The galaxy density enhancement associated with this system extends for $\gtrsim 100h^{-1}$ Mpc (the Hubble constant is $H_0 = 100h$ km s⁻¹Mpc⁻¹).

The Schechter (1976) luminosity function parameters for the CS are: $M_{CS}^* = -20.73_{-0.18}^{+0.17}$, $\alpha_{CS} = -1.17_{-0.19}^{+0.19}$, and $\phi_{CS}^* = 0.0250 \pm 0.0061$ Mpc⁻³mag⁻¹. In concert with the ESO Key Program (Vettolani et al., 1997; Zucca et al., 1997) and the AUTOFIB (Ellis et al., 1996) surveys, the CS indicates that the absolute normalization of the luminosity function exceeds estimates based on shallower and/or sparser surveys.

¹Work reported here based partly on observations obtained at the Michigan-Dartmouth-MIT Observatory

²Work reported here based partly on observations at the Multiple Mirror Telescope, a joint facility of the Smithsonian Institution and the University of Arizona

³Now at Observatories of the Carnegie Institution of Washington, Pasadena, CA 91101

Subject headings: Galaxies: Surveys Galaxies: Distances and redshifts
Galaxies: Luminosity function Cosmology: Observations Cosmology:
Large-Scale structure of the universe

1. Introduction

The “Century Survey” (CS) is a complete redshift survey of 102 square degrees to a limiting $m_R = 16.13$ containing 1762 galaxies. It complements the suite of sparse surveys to comparable or greater depth (Loveday et al., 1992: APM ;Shectman et al., 1996 : LCRS). The sample size is comparable with that of the much deeper, complete ESO Key Program of 23.3 square degrees (Vettolani et al., 1997; Zucca et al., 1997 : ESO-KP). The CS covers the central 1° -wide declination range of the first slice of the CfA survey (de Lapparent et al., 1986). In the northern hemisphere, the CS is the largest complete survey to its depth.

The qualitative features of the survey (Plate 1) are similar to the structures in other large redshift surveys (Geller and Huchra 1989; Giovanelli and Haynes 1989; da Costa et al., 1994; Shectman et al., 1996; Vettolani et al., 1997). The survey slices through a number of large voids and dense, coherent, thin walls (including a portion of the Great Wall). An outer region of the Coma cluster ($\alpha = 12^{\text{h}}57.5^{\text{m}}, +28^\circ15'$, $cz = 6850 \text{ km s}^{-1}$; Colless and Dunn 1996) and a portion of the classical Corona Borealis supercluster ($\alpha = 15.3 - 15.6^{\text{h}}, \delta = 27.5 - 32^\circ$; see Postman et al., 1988; Small et al., 1997) lie within the CS: these regions contribute prominent “fingers” in redshift space. Note that throughout this paper we use B1950 coordinates.

Like the CfA and SSRS2 surveys, the CS is complete to its magnitude limit. Although they cover more than a third of the sky, the CfA and SSRS2 surveys contain structures which extend across most of the sample volume. One might expect that because of the greater depth of the CS, individual large features (like the Great Wall) would be less likely to dominate its large-scale structure statistics. However, the $12,800 \text{ km s}^{-1}$ scale claimed by Broadhurst et al. (1990) and the excess power on a scale of $\sim 100h^{-1} \text{ Mpc}$ in the LCRS (Landy et al., 1996) suggest caution (see Section 2b). In fact, within the CS, we find further evidence for inhomogeneity on a $\sim 100h^{-1} \text{ Mpc}$ scale.

Here we display the data and discuss the first analyses of the CS. Section 2 describes the survey. In Section 3 we compute the R -band luminosity function for the entire survey. We also examine the variation of the galaxy number density with redshift. We conclude in Section 4.

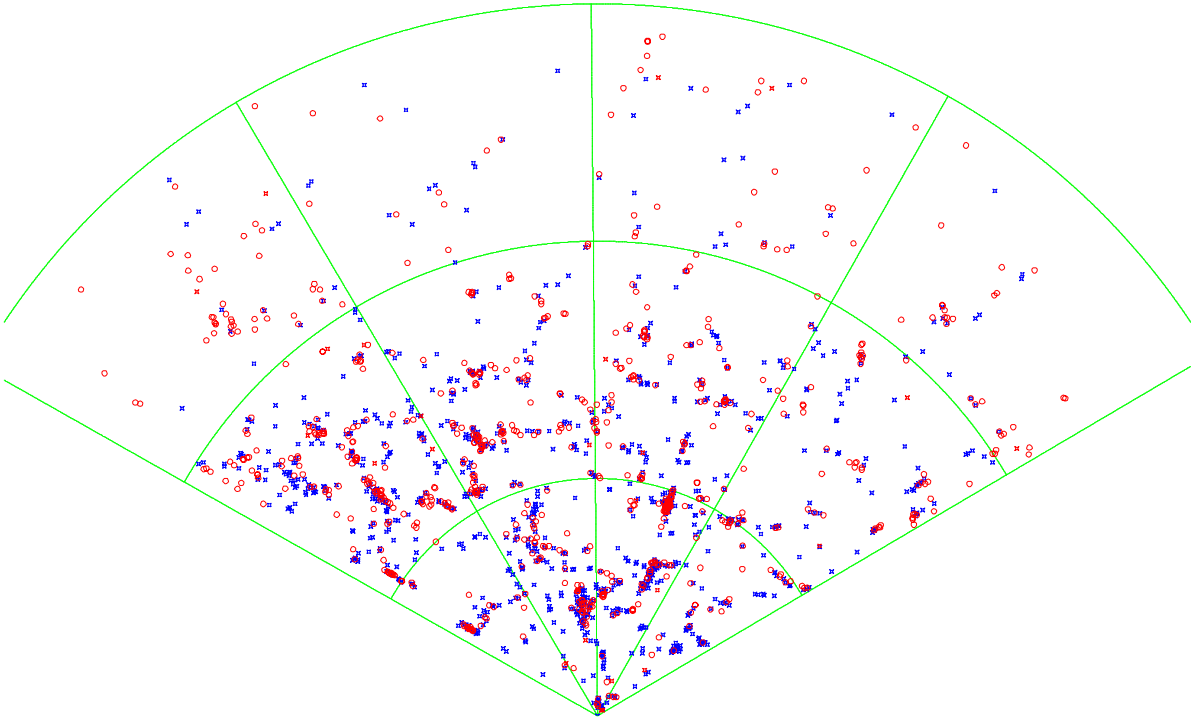


Fig. Plate 1.— Cone diagram for the Century Survey. The right ascension runs from 8.5^h to 16.5^h and the radial green lines are at 2 hour intervals. The outer boundary of the plot is at 45,000km s⁻¹ and the green lines at constant velocity mark 15,000 km s⁻¹ intervals. Blue points represent spiral galaxies; yellow ones are early types. In the gray-green regions there is a mix of types.

2. The Galaxy Distribution

2.1. The Data

The CS is a complete photometric and spectroscopic survey of the region $8^{\text{h}}30^{\text{m}} \leq \alpha \leq 16^{\text{h}}20^{\text{m}}$ and $29^\circ \leq \delta \leq 30^\circ$. The spectroscopic survey is 98.4% complete to $m_R = 16.13$ over the entire right ascension range. We are 99.4% complete to $m_R = 16.4$ over the right ascension range $8^{\text{h}}32^{\text{m}}$ to $10^{\text{h}}45^{\text{m}}$. In this deeper sample, there are 518 galaxies; 177 of these have $m_R \leq 16.13$. Here we discuss the sample complete to $m_R = 16.13$. Kurtz et al. (1997) discuss the deeper sample.

We constructed the galaxy catalog from scans of the POSS E plates according to the procedures outlined by Kurtz et al. (1985). For each galaxy in the catalog we derive an isophotal magnitude to a bright limiting isophote which varies unavoidably from plate to plate. Two drift scans from $8^{\text{h}}27^{\text{m}}$ to $11^{\text{h}}55^{\text{m}}55^{\text{s}}$ and from $11^{\text{h}}50^{\text{m}}$ to $15^{\text{h}}45^{\text{m}}$ provide the magnitude calibration (Ramella et al., 1995; Kent et al., 1993). The drift scans are both centered at $\delta = 29.5^\circ$. The drift scan for early α 's was done with the 1.2-m telescope and for late α 's with the 61-cm telescope (now retired) of F. L. Whipple Observatory (FLWO). We used pointed observations to calibrate the three POSS plates E924, E1365, and E134 which cover the right ascension ranges $8^{\text{h}}32^{\text{m}}32^{\text{s}}$ to $8^{\text{h}}58^{\text{m}}50^{\text{s}}$ and $15^{\text{h}}53^{\text{m}}$ to $16^{\text{h}}19^{\text{m}}44^{\text{s}}$ (see the next paragraph). Calibration details are in Kurtz et al. (1997).

As a function of right ascension, Figure 1 (lower panel) shows the difference, $\Delta_{\text{drift}} = m_D - m_{DCCS}$, between the drift scan magnitudes, m_D , and the drift-scan calibrated CS, m_{DCCS} , for the 457 galaxies in common. To calibrate each plate, we set the median $\Delta_d = 0$. The overall average is $\Delta_{\text{drift}} = 0.018 \pm 0.014$ and the rms scatter about the mean is 0.29^{m} .

To check the drift scan calibration we acquired more than 200 pointed observations with the MDM 2.4-m and 1.3-m telescopes under photometric conditions. The photometry for these observations is better than 3% in all cases. Comparison of these large aperture pointed magnitude measurements with the drift scans demonstrates that there are no systematic zero-point variations across either drift (see Kurtz et al. 1997 for further details). Figure 1 (upper panel) shows the difference between 92 pointed photometric observations and the drift-scan calibrated CS as a function of right ascension. Except for three plates noted above (where we calibrate with these pointed observations only), the pointed photometry provides an independent check of the CS drift scan calibration. The rms scatter in $\Delta_{\text{ccd}} = m_p - m_{DCCS}$ is 0.19^{m} and the median zero-point offset is $0.015^{\text{m}} \pm 0.02^{\text{m}}$. The m_p 's are the magnitudes for the pointed observations. The scatter here is an underestimate of the error in the CS photometry because we have not made a detailed accounting of the

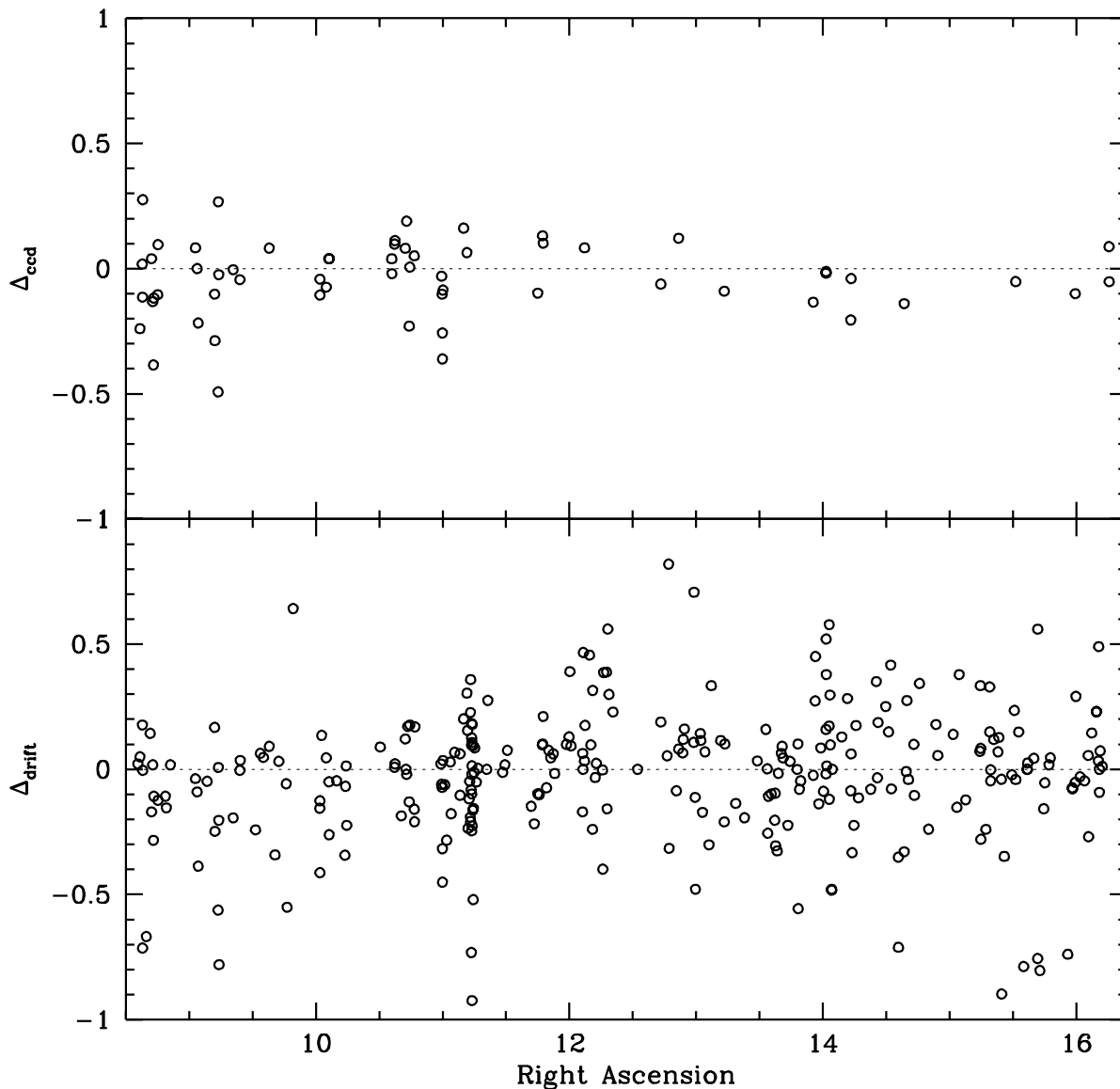


Fig. 1.— CS photometry. The upper panel shows the difference between the pointed photometric observations and the drift-scan calibrated CS as a function of right ascension. The lower panel shows the difference between the drift scan magnitudes and the drift-scan calibrated CS as a function of right ascension. Note that we do not use the drift scan data for calibration in the right ascension ranges $8^{\text{h}}32^{\text{m}}32^{\text{s}}$ to $8^{\text{h}}58^{\text{m}}50^{\text{s}}$ and $15^{\text{h}}53^{\text{m}}$ to $16^{\text{h}}19^{\text{m}}44^{\text{s}}$.

photometric errors for objects which are not cleanly separated from their neighbors. Based on these considerations, we take 0.25^m as the standard error in the CS magnitudes.

There are 1762 galaxies with $m_R \leq 16.13$. Only 28 of these do not have measured redshifts. Most of the galaxies without redshift measurements are near the limiting magnitude and their inclusion in the survey is largely a result of final refinement of the magnitude calibration. We measured 1467 new redshifts; we measured 631 of these with the Decaspec (Fabricant and Hertz 1990) mounted on the MDM 2.4-meter. In sparser regions, where the ten-fiber probe Decaspec would have been ineffective, we measured 774 redshifts either with the blue channel of the MMT spectrograph (with image intensified Reticon detectors) or with the red or blue channel MMT spectrograph (equipped with CCD detectors). The remaining redshifts are from single-slit 2.4-meter measurements or from FAST spectrograph (Fabricant et al., 1997) observations at the 1.5-meter Tillinghast at FLWO. Previously published redshifts in this region are from Huchra et al. (1990; 164 redshifts), Thorstensen et al. (1989; 92 redshifts), and Willmer et al. (1996; 11 redshifts).

We extracted redshifts from all of the absorption-line spectra according to the cross-correlation procedure of Tonry and Davis (1979). For emission-line spectra from MDM and from the MMT spectrograph, we derive redshifts with a multiple-gaussian fitting routine. For the more recent MMT red and blue channel data, we used the cross-correlation technique for both emission- and absorption-line spectra. At Dartmouth, we used the REDUCE/INTERACT package (Maker et al., 1982) to extract redshifts; at the CfA we used EMSAO and XCSAO (Kurtz and Mink 1997). For all of the data, the typical error in the velocities is 70 km s^{-1} . From 67 measurements in common, the zero-point offset between the MDM and MMT data is $1.2 \pm 6.3 \text{ km s}^{-1}$.

One of us (G. Wegner) used a 30 power loupe to obtain Hubble types from glass copies of the POSS1 O-plates (the coarse classification bins are E, S0, Sa, Sb, Sc, Irr and the corresponding barred types) for all of the galaxies with $m_R \leq 16.13$. From galaxies which appear on more than one plate, we estimate that the classification error is ± 1 type. The median type in this R -selected survey is Sa. We describe and analyze the classifications in much greater detail in Kurtz et al. (1977).

We make two corrections to the computed absolute magnitudes:

$$M(m, z, T) = m - 5 \log D_L(z) - 25 - K_T(z) - A_R$$

where m is the apparent R magnitude from the photometric catalog, D_L is the luminosity distance in megaparsecs at redshift z , K_T is the R -band K -correction for Hubble type T , and A_R is the extinction at R . We correct for Galactic extinction using the reddening

maps of Burstein and Heiles (1982) and a ratio of total to selective absorption of $R_R = 2.3$. The majority of the survey galaxies lie at high Galactic latitude; the largest absorption correction is 0.09 magnitudes. We determine K-corrections for each galaxy type using the spectral synthesis models of Rocca-Volmerange and Guiderdoni (1988). At the chosen redshift limit of the survey, $cz = 45,000 \text{ km s}^{-1}$, these K-corrections range from -0.02 magnitudes for irregulars to 0.2 magnitudes for ellipticals. We compute distances directly from the galaxy redshifts in the Local Group frame:

$$D_L(z) = \frac{c}{H_0}(1+z)Z_q(z)$$

$$Z_q(z) = \frac{1}{q_0^2(1+z)}\{q_0z + (q_0 - 1)[(1 + 2q_0z)^{1/2} - 1]\}$$

where $cz = cz_\odot + 300 \sin l \cos b$. To facilitate comparisons with earlier work, we use $H_0 = 100h \text{ km s}^{-1}\text{Mpc}^{-1}$ with $h = 1$. We assume a mass density $\Omega_0 = 0.3$ (consistent with several recent measurements) and zero cosmological constant: thus the deceleration parameter is $q_0 = 0.15$.

2.2. The Redshift Map

Plate 1 shows the distribution of the CS galaxies with $cz \leq 45,000 \text{ km s}^{-1}$ color-coded by morphological type. Blue signifies types Sa and later; yellow corresponds to the early types E and S0. Regions occupied by both early and late types are gray-green.

Three qualitative results are evident in the map. First, both early- and late-type galaxies trace the large-scale features in the survey. This result is also evident in the two slices of the CfA2 survey for which types are available (Huchra et al., 1990; Huchra et al., 1995). Second, the few galaxies within the lowest density regions (voids) tend to be of late-type, but there are *some* E's and S0's. In a shallower survey of the first CfA slice, Thorstensen et al. (1995) also noted the presence of early-type galaxies in low density regions.

Finally, the cores of rich clusters are rich in early-type galaxies. Portions of the central fingers appear dark green in Plate 1 because the cores are surrounded by late-type galaxies (a few are within the core) which generally have a more extended distribution also visible in Plate 1. The superposition of early and late types at the same position produces the gray-green dots. These effects are already well known from detailed studies of individual

clusters (Colless and Dunn 1996; Mohr et al., 1996; Carlberg et al., 1997).

The CS contains portions of 7 Abell clusters (A690, A1185, A1213, A1656, A2079, A2162, and A2175). The prominent “finger” at $\sim 13^{\text{h}}$ is part of the Coma cluster; its center is south of the survey boundary at $28^{\circ}15'$.

The cluster A2079 ($15^{\text{h}}26^{\text{m}}$, $29^{\circ}15'$, $cz = 19,600 \text{ km s}^{-1}$) is one of the six clusters in the classical Corona Borealis supercluster (Cor Bor). The other five clusters (A2061, A2065, A2067, A2089, and A2092) are outside the declination range of the CS. These systems span the right ascension range $15.3^{\text{h}} - 15.6^{\text{h}}$ and the approximate velocity range $18,000 - 25,000 \text{ km s}^{-1}$ (Postman et al., 1988; Small et al., 1997). In this velocity range, the CS is surprisingly dense all the way from 14.5^{h} to 16.5^{h} . At the median redshift of Cor Bor ($cz \sim 22,000 \text{ km s}^{-1}$, which also happens to be the depth, D^* , to which an L^* galaxy is brighter than the magnitude limit), the dense region has an extent of $\sim 100h^{-1} \text{ Mpc}$, comparable with the scale where excess power is detected in the Las Campanas Redshift Survey (LCRS; Landy et al., 1996).

Counts in the cells marked in Plate 1 give a measure of the extent of Cor Bor and of its contrast with other portions of the CS. In the easternmost cell with velocity range $15,000$ to $30,000 \text{ km s}^{-1}$, there are 348 galaxies (only 92 of these are in the canonical $15.3 - 15.6^{\text{h}}$ Cor Bor range). In this velocity range the counts in the other three cells from east to west are, respectively: 214, 184, and 141. In the cell which contains Cor Bor, the galaxy number density is ~ 1.7 times the overall median. The east-west gradient does not persist throughout the velocity range of the survey and thus it is not a result of an undiscovered systematic error in the photometry. In fact, we compute (Section 3) the luminosity function parameters for the eastern and western halves of the survey; all three parameters (the amplitude, characteristic luminosity, and faint-end slope) are indistinguishable at the 1σ level.

3. The Luminosity Function

There are several recent surveys containing $\gtrsim 1000$ galaxies which yield determinations of the local luminosity function. They include Loveday et al. (1992: APM), Marzke et al. (1994a,b: CfA2), da Costa et al. (1994: SSRS2), Shectman et al. (1996: LCRS), Ellis et al. (1996: AUTOFIB), and Zucca et al. (1997: ESO-KP). The APM, CfA2, SSRS2, AUTOFIB, and ESOKP are all blue-selected surveys. Like the CS, the LCRS is red-selected (at Gunn r rather than at the Kron-Cousins R we use; $r - R = 0.35$; Jorgensen 1994). There should be some variation in the *shape* of the luminosity function with color because of the

expected associated change in morphological mix. The CS luminosity function parameters are thus most directly comparable with the LCRS. For comparison with b_J -selected surveys, the median is $(b_J - R_{KC}) = 1.3$ for the CS mix of morphological types (Buta et al., 1995; Buta and Williams 1995).

We use the STY maximum-likelihood (Sandage et al., 1979; Yahil et al., 1991) and stepwise maximum likelihood (Efstathiou et al., 1988 : SWML) techniques to determine the parameters M^* and α in the Schechter (1976) function:

$$\phi(M) = 0.4 \ln 10 \phi^* [10^{0.4(M^* - M)}]^{(1+\alpha)} \exp[10^{0.4(M^* - M)}]. \quad (1)$$

Both methods are inhomogeneity-independent. We assume that the luminosity function is independent of position. Thus we can determine its form and amplitude, ϕ^* , separately. The STY method is parametric; the SWML method provides a measure of the goodness of fit for the STY parameters, M^* and α .

The *observed* luminosity function $\phi(M)$ is a convolution of the magnitude error distribution with the *true* luminosity function of equation (1). We assume that the magnitude error distribution is Gaussian with a dispersion of $\sigma_M = 0.25$.

We construct the luminosity function for $1,000 \text{ km s}^{-1} \leq cz \leq 45,000 \text{ km s}^{-1}$. The lower limit eliminates regions where peculiar velocities may be a large fraction of the cosmological recession velocity; the upper limit is where the survey becomes too sparse to be useful.

Figure 2 shows the binned STY (curve) and SWML (symbols with error bars) estimates of the *observed* (convolved) luminosity function for the entire CS sample. Inversion of the information matrix yields the error bars on the SWML estimates (Efstathiou et al., 1988). Marzke et al. (1994a) describe this approach in detail.

The inset in Figure 2 shows the 1σ error ellipse for the Schechter (1976) function parameters, $M_{CS}^* = -20.73_{-0.18}^{+0.17}$ and $\alpha_{CS} = -1.17_{-0.19}^{+0.19}$ derived from the STY technique. With $r - R = 0.35$, M_{CS}^* is coincident with M_{LCRS}^* (Table 1; the open box within the inset shows the best-fit LCRS parameters). However, the CS faint-end slope is significantly ($\sim 2.5\sigma$) steeper than $\alpha_{LCRS} = -0.70 \pm 0.05$. The source of this discrepancy is unclear. One possibility is that the selection criteria used in the LCRS bias the survey against the faintest galaxies. Because of the correlation between absolute magnitude and surface brightness, the central surface-brightness cut in the LCRS is the criterion most likely to eliminate galaxies from the faint end of the LF. The effect may, in fact, be small, but it remains to be evaluated. Although our survey (as any magnitude-limited survey) is biased to high surface brightness galaxies as well (Kurtz et al. 1997), we avoid explicit cuts on

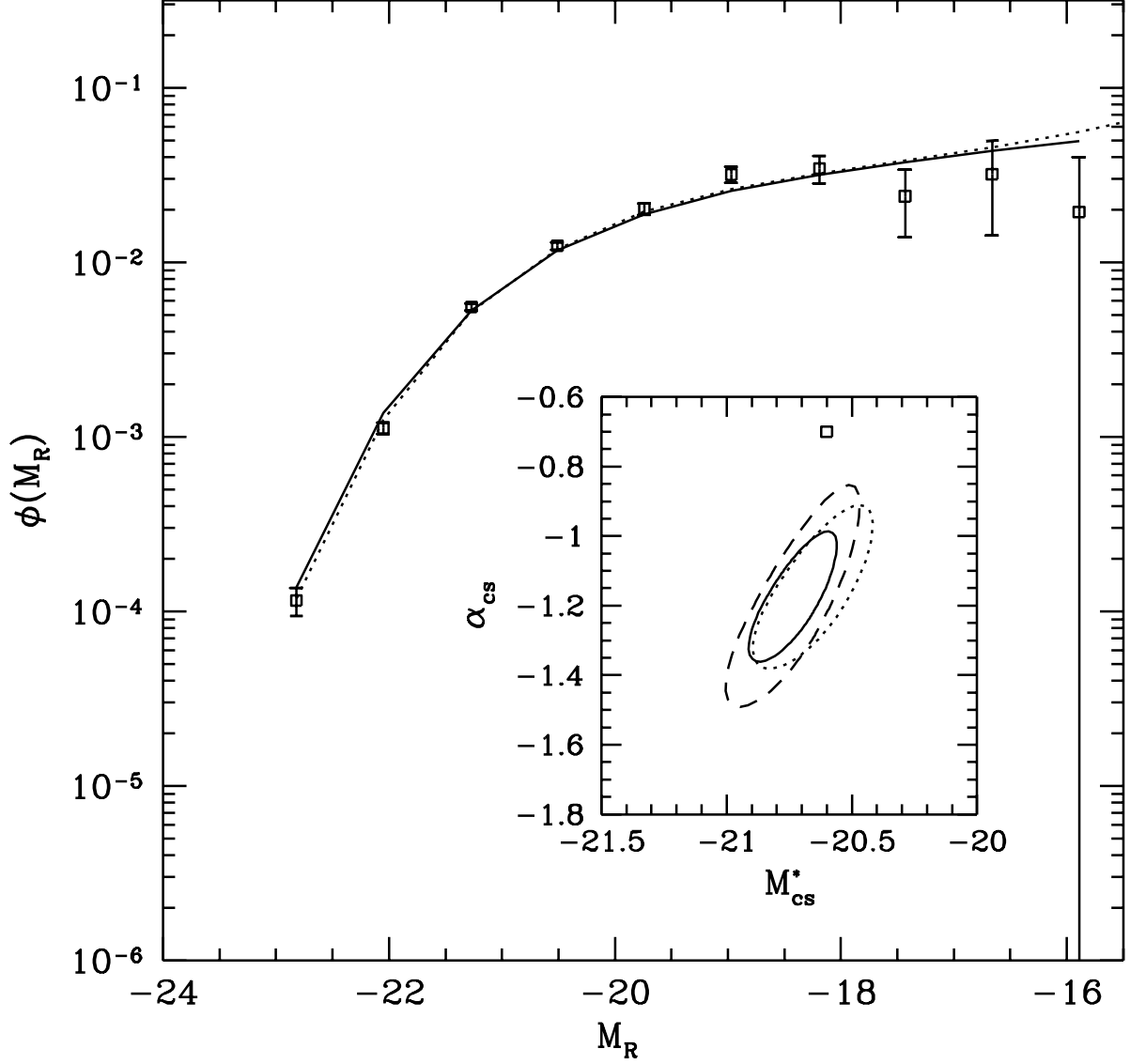


Fig. 2.— The CS luminosity function. The points with error bars are the SWML estimates. The solid curve is the STY fit with the parameters listed in Table 1. The dotted curve is the R -band luminosity function predicted from the B -band SSRS2. The STY fit is based on galaxies with $1,000 < cz \leq 45,000 \text{ km s}^{-1}$. The inset shows the 1σ error ellipses for the luminosity function parameters for the entire survey (solid), the East half (dashed), and the West half (dotted). The open box shows the best fit for the LCRS.

anything but apparent R magnitude. This difference in survey strategy between the CS and the LCRS may contribute to the discrepancies at the faint end of the LF.

Although the LCRS slope differs significantly from the one we measure, comparable surveys in other passbands yield results which are quite consistent with ours. In particular, our α_{CS} is indistinguishable from the faint end slopes measured in the ESOKP (Zucca et al. 1997) and in the AUTOFIB surveys (Ellis et al. 1996, for the regime $0.02 < z < 0.15$), both of which are selected in b_J .

The agreement between our R -selected survey and recent blue-selected surveys would be surprising if the early-type luminosity function were radically different from the late-type luminosity function. In the very local B -selected samples, the early-type luminosity function is essentially indistinguishable from the spiral luminosity function (SSRS2:Marzke et al. 1997, CfA2: Marzke et al. 1994). At redder wavelengths, the luminosity function of red, early-type galaxies must then be brighter than the luminosity function of blue, late types. Because late types outnumber early types by a factor of nearly two, the overall luminosity function develops a feature around the knee in bandpasses where the color differential between early and late types exceeds a magnitude or so. In the R band, the color difference between ellipticals and Sbc's is only half a magnitude. The net effect is that in the R -band, the early-type galaxies determine M^* ; late types still govern the faint-end.

The dotted curve in Figure 2 shows the R -band luminosity function predicted from the B -selected SSRS2 luminosity function. Marzke et al. (1997) divide the SSRS2 luminosity function into three type bins: E/S0, Spiral and Irregular. The SSRS2 luminosity function parameters are (Marzke et al. 1997) : E/S0 , $M^* = -19.42^{+0.10}_{-0.11}$, $\alpha = -1.03^{+0.09}_{-0.09}$, $\phi^* = 4.3 \pm 0.8 \times 10^{-3} \text{ Mpc}^{-3}$; Spiral, $M^* = -19.46^{+0.07}_{-0.08}$, $\alpha = -1.11^{+0.07}_{-0.07}$, $\phi^* = 8.1 \pm 1.3 \times 10^{-3} \text{ Mpc}^{-3}$; Irregular, $M^* = -19.72^{+0.41}_{-0.52}$, $\alpha = -1.86^{+0.25}_{-0.26}$, $\phi^* = 0.2 \pm 0.1 \times 10^{-3} \text{ Mpc}^{-3}$. For a basic model, we translate these B -selected luminosity functions to the R band using the mean $B - R$ colors from Frei and Gunn (1995). We do not account for the large intrinsic scatter in the color for each morphology. For ellipticals, Sbc's (roughly the mean spiral type in SSRS2) and irregulars, the colors are 1.39, 0.95 and 0.57, respectively. We adjust the normalization by the ratio of ϕ_{*CS}/ϕ_{*SSRS2} to compare the shapes directly. The predicted R -band luminosity function agrees remarkably well with the CS luminosity function.

Gardner et al. (1997) determined the galaxy luminosity function for a K-band survey. Here too, the faint-end slope, $\alpha = -0.91 \pm 0.2$, is nearly flat. Because late spirals and ellipticals differ in $B - K$ by more than two magnitudes, the early and late-type luminosity functions are well separated at K . The composite luminosity function may reflect this separation.

We also compute luminosity functions for the east and west halves of the photometric CS (the division is at $\alpha = 12^{\text{h}}56^{\text{m}}18^{\text{s}}$). To within the errors, all of the luminosity function parameters for the subsamples and for the survey as a whole are similar. The inset of Figure 2 shows the error ellipses for the East (dashed) and West (dotted) samples. The nearly complete overlap demonstrates the consistency of the photometry across the survey. Table 1 lists the number of galaxies used to compute the luminosity function for each sample.

To compute the luminosity function amplitude, ϕ_{CS}^* , we use the minimum variance estimator derived by Davis and Huchra (1982). Figure 3 shows the behavior of ϕ_{CS}^* as a function of velocity. The Cor Bor region (Section 2b) causes the peak at $\sim 24,000 \text{ km s}^{-1}$. The peak centered at $9,000 \text{ km s}^{-1}$ is the Great Wall, bounded by a few large voids in its foreground and background. Examination of Plate 1 shows that the fluctuations at $cz \leq 16,000 \text{ km s}^{-1}$ result from a small number of large-scale features.

In Figure 3, the points with error bars are the estimates based on the best-fit luminosity function parameters for the entire sample in Table 1. The error bars are the formal error in the estimator. The boundaries of the shaded region show the behavior of ϕ_{CS}^* at the extrema of the error ellipse in Figure 2.

The luminosity function fit is most sensitive to the galaxies with magnitudes near M_{CS}^* . In Table 1 we therefore quote the average ϕ_{CS}^* for the velocity range [18,000:28,000] centered on the velocity ($22,000 \text{ km s}^{-1}$) where an M_{CS}^* galaxy is at the magnitude limit of the survey. The vertical dotted lines in Figure 3 mark this range which includes 653 galaxies. The result, $\phi_{CS}^* = 0.0250 \pm 0.0061 \text{ Mpc}^{-3} \text{ mag}^{-1}$, agrees very well with the ESOKP and AUTOFIB surveys and is within 1σ of the LCRS value. Our error is large because of the fluctuation induced by Cor Bor (see Section 2.2). The difference in ϕ^* between the east and west halves of the sample, though not formally significant, is in the sense expected from the presence of Cor Bor in the east half.

To examine the dependence of ϕ_{CS}^* (or, equivalently, galaxy density) on velocity, we divide the sample into three velocity bins: [1,000: 18,000], [18,000: 28,000], and [28,000:45,000] marked in Figure 3. The value of ϕ_{CS}^* is quite sensitive to the form parameters, M^* and α . To examine this sensitivity for each velocity range, we compute the median value of ϕ_{CS}^* and of the boundaries of the 1σ error region for the form parameters (Figure 2). The values of M^* and α are fixed throughout the entire velocity range. For the successive velocity intervals, the ranges of ϕ^* are: (0.015, **0.017**, 0.021); (0.021, **0.027**, 0.034) and (0.014, **0.025**, 0.049). The boldface values are the median ϕ_{CS}^* . The other two numbers are the median value for the lower and upper boundaries of the shaded region.

These estimates of ϕ_{CS}^* suggest, albeit with modest significance, that the mean galaxy

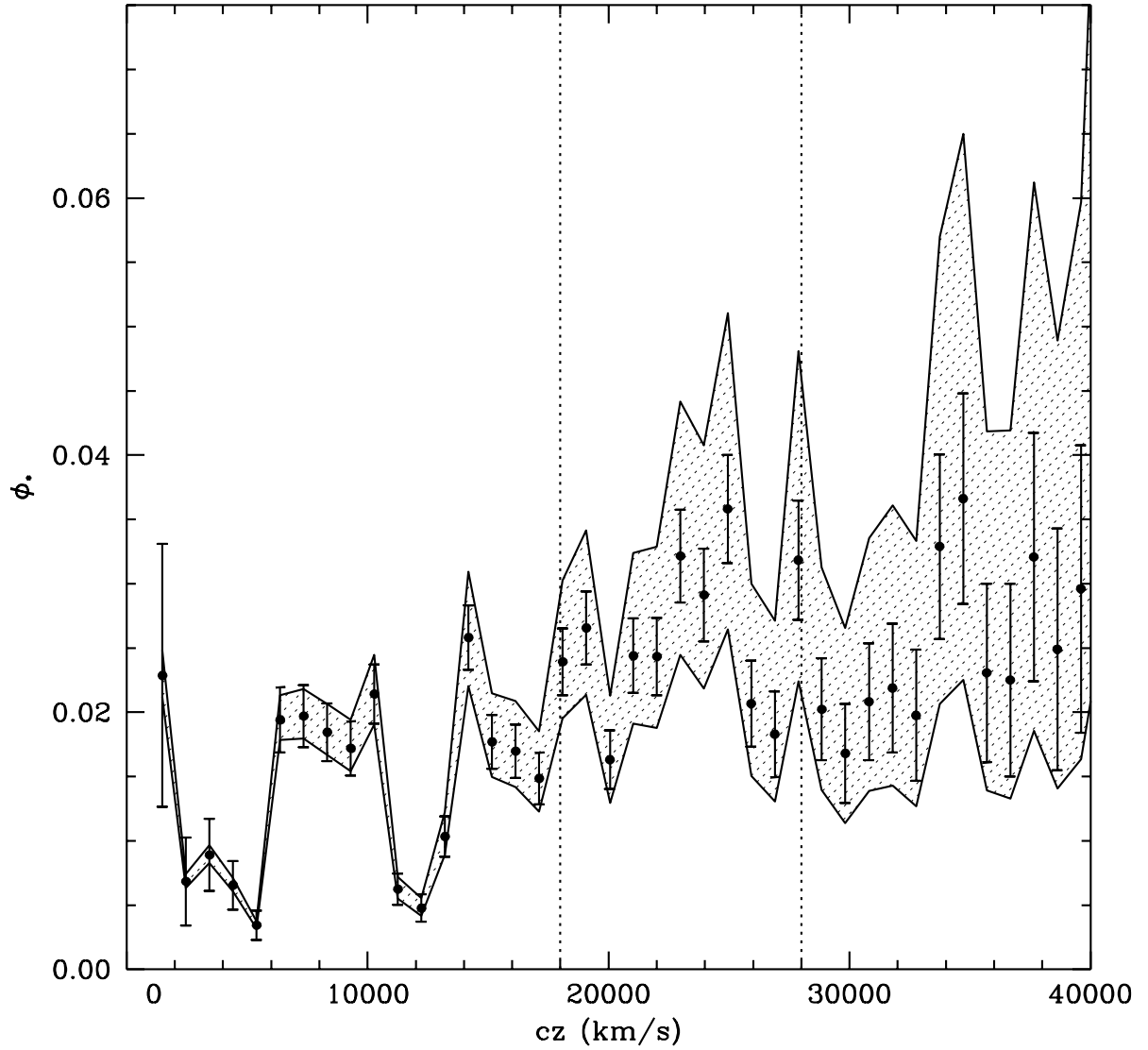


Fig. 3.— Absolute normalization for the Century Survey luminosity function. The points with error bars are the best estimates. The boundaries of the dotted region are the results for the extrema of the error ellipse in Figure 2. The vertical dotted lines indicate the ranges for computation of the median ϕ_* .

density is low nearby and rises by 50% for $cz \gtrsim 18,000 \text{ km s}^{-1}$. The amplitude for $cz \gtrsim 18,000 \text{ km s}^{-1}$ agrees very well with the results of the AUTOFIB survey. The behavior of ϕ_{CS}^* is similar to that of the ESO-KP (Table 1). On the other hand, the 1σ limits provide a cautionary note. They show that the CS admits either a constant density or a steadily increasing one and underscore the sensitivity of the behavior of ϕ^* to the form parameters of the luminosity function. Any survey errors in M^* comparable with the CS errors would presumably show similar behavior.

The CS samples a region of the universe completely disjoint from those sampled by the other surveys to comparable depth. Like other recent redshift surveys to comparable depth, the CS indicates that the sparse APM survey and shallower surveys like the SSRS2 underestimate the absolute normalization of the galaxy luminosity function. This local underestimate probably results from large-scale structure, but the details remain unclear. The CS (and other surveys) do show that there *are* galaxy density enhancements (like Cor Bor) which exceed the mean galaxy density by $\sim 70\%$ on a scale of $\sim 100h^{-1} \text{ Mpc}$. A local underdensity on a comparable scale would explain the results.

4. Conclusion

Comparison of the CS luminosity function with other surveys presents an interesting, if somewhat puzzling, picture. The luminosity function parameters, M^* and ϕ^* , are in agreement with the LCRS and with dense b_J -selected surveys to comparable depth. However, the faint-end slope for the LCRS is shallower than the CS, and the b_J -selected surveys. It is encouraging that we can predict the CS R -band luminosity function from the much shallower SSRS2 B -band survey.

The CS is complete to the magnitude limit and requires no sampling corrections. For the other surveys listed in Table 1, the luminosity function computation requires some correction for incompleteness. These corrections are smallest for the ESO-KP and AUTOFIB. In concert with the ESO-KP and AUTOFIB surveys, the CS indicates that the absolute normalization of the luminosity function exceeds estimates based on shallower and/or sparser surveys.

The LCRS indicates that there are inhomogeneities in the galaxy distribution on a scale of $100h^{-1} \text{ Mpc}$. The Century Survey covers too small a volume to provide a comparable measure, but it does cross the Corona Borealis supercluster. This system is embedded in a dense region much more spatially extensive than the classical supercluster. The galaxy number density exceeds the mean by $\sim 70\%$ on a scale of $\sim 100h^{-1} \text{ Mpc}$.

Underdense regions on this scale might account for the low estimates of the luminosity function normalization at low redshift.

The CS data include spectroscopic types and galaxy morphologies. Kurtz et al. (1997) will discuss the dependence of the luminosity function on these characteristics. This paper will also include an analysis of the portion of the CS sample with $m_R \leq 16.4$. Subsequent papers on the CS will include 1) an analysis of the low-order moments of the pairwise velocity distribution and 2) a data paper which includes all of the spectroscopic and photometric data.

We thank Steve Kent and Massimo Ramella for providing their drift scan data to calibrate our survey. Mario Nonino generously helped us to understand the drift-scan data. Carol Heller, John McAfee, and Janet Miller provided expert assistance in making the MMT observations. We thank Shoko Sakai for making some of the MDM 2.4-meter observations and Bob Barr for his excellent support at the 2.4-meter. We thank Susan Tokarz for reducing the MMT and 1.5-meter data and we thank Jim Peters and Perry Berlind for making the 1.5-meter observations. We thank Peter Challis and Robert Kirshner for measuring a small number of redshifts at the MMT to help make the survey complete. We thank the referee, Richard Ellis, for leading us to consider the relationship between R- and B-band luminosity functions in more detail.

At the CfA, this research was supported in part by NASA Grant NAGW-201 and by the Smithsonian Institution. We thank Irwin Shapiro for providing substantial funding for the construction of the Decaspec at the CfA. Edward Hertz did the skillful, dedicated Decaspec engineering. At Dartmouth, JRT was supported in part by NSF grant AST 86-20081 and by a Research Corporation Cottrell Grant; GW was supported in part by NSF grants AST86-20081, AST90-23450, and AST93-47714. Dean Bruce Pipes provided partial financial support for the construction of the Decaspec.

Table 1. Luminosity Function Parameters

Sample	N_{gal}	$M^*(R_{KC})$	α	$\phi^*(\times 10^{-3} \text{ Mpc}^{-3})$	notes
Century-All	1695 ^a	$-20.73_{-0.18}^{+0.17}$	$-1.17_{-0.19}^{+0.19}$	25.0 ± 6.1	...
Century-East	846 ^a	$-20.78_{-0.29}^{+0.25}$	$-1.20_{-0.31}^{+0.32}$	32.1 ± 11.1	...
Century-West	849 ^a	$-20.68_{-0.26}^{+0.22}$	$-1.15_{-0.24}^{+0.23}$	21.4 ± 12.2	...
LCRS	18678	$-20.64_{-0.02}^{+0.02}$	$-0.70_{-0.05}^{+0.05}$	19.0 ± 1.0	$(r - R_{KC}) = 0.35$
ESO-KP	3342	$-20.91_{-0.08}^{+0.06}$	$-1.22_{-0.07}^{+0.06}$	20.0 ± 4.0	$(b_j - R_{KC}) = 1.30$
AUTOFIB	588	$-20.60_{-0.12}^{+0.15}$	$-1.16_{-0.05}^{+0.05}$	$24.5_{-3.1}^{+3.7}$	$(b_j - R_{KC}) = 1.30$

^a α and M^* are based on this sample size; ϕ^* is based on the subset in the 18,000 – 28,000 km/s range; 653(All), 246(West), 407(East)

REFERENCES

- Broadhurst, T.J., Ellis, R.S., Koo, D., Szalay, A.S. 1990, *Nature*, 343, 726.
- Burstein, D. and Heiles, C. 1982, *AJ*, 87, 1165.
- Buta, R., Corwin, H.G., de Vaucouleurs, G., de Vaucouleurs, A., Longo, G. 1995, *AJ*, 109, 517.
- Buta, R. and Williams, K.L. 1995, *AJ*, 109, 543.
- Carlberg, R.G., Yee, H.K.C., Ellingson, E., Morris, S.L., Abraham, R., Gravel, P., Pritchett, C.J., Smecker-Hane, T., Hartwick, F.D.A., Hesser, J.E., Hutchings, J.B. and Oke, J.B. 1997, *ApJ*, 476, L7
- Coleman, G.D., Wu, C-C. and Weedman, D.W. 1980, *ApJ*, 43, 393.
- Colless, M. and Dunn, A.M. 1996, *ApJ*, 458, 435.
- da Costa, L.N., Geller, M.J., Pellegrini, P.S., Latham, D.W., Fairall, A.P., Marzke, R.O., Willmer, C.N.A., Huchra, J.P., Calderon, A.P., Ramella, M., and Kurtz, M.J. 1994, *ApJ*, 424, L1.
- Davis, M. and Huchra, J.P. 1982, *ApJ*, 254, 437.
- de Lapparent, V. , Geller, M.J., and Huchra, J.P. 1986, *ApJ*, 302, L1.
- Ellis, R.S., Colless, M., Broadhurst, T., Heyl, T. and Glazebrook, K. 1996, *MNRAS*, 280,235.
- Efstathiou, G., Ellis, R.S., and Peterson, B.A. 1988, *MNRAS*, 280, 25.
- Fabricant, D.G. and Hertz, E. 1990, *Proc. SPIE*, 1235, 747.
- Fabricant, D.G., Cheimets, P., Caldwell, N. and Geary, J. 1997, *PASP*, in press.
- Frei, Z. and Gunn, J.E. 1994,*AJ*, 108, 1476.
- Geller, M.J. and Huchra, J.P. 1989, *Science*, 246, 897.
- Giovanelli, R. and Haynes, M.P. 1989, *AJ*, 97, 633
- Huchra, J.P., Geller, M.J., de Lapparent, V. and Corwin, H. 1990, *ApJS*, 72, 433.
- Huchra, J.P. Geller, M.J. and Corwin, H.J. 1995, *ApJS*, 99, 391.

- Jorgensen, I. 1994, PASP, 106, 967.
- Kent, S.M., Ramella, M. and Nonino, M. 1993, AJ, 105, 393.
- Kurtz, M.J., Huchra, J.P., Beers, T.C., Geller, M.J., Gioia, I.M., Maccacaro, T., Schild, R.E., Stauffer, J.R. 1985, AJ, 90, 1665.
- Kurtz, M.J. and Mink, D. 1997, in preparation.
- Kurtz et al. 1997, in preparation.
- Landy, S.D., Shectman, S.A., Kirshner, R.P., Oemler, A., Tucker, D. 1996, ApJ, 456, L1.
- Lin, H., Kirshner, R.P., Shectman, S.A., Landy, S.D., Oemler, A., Tucker, D.L., Schechter, P.L. 1996, ApJ, 464, 60.
- Loveday, J., Peterson, B.A., Efstathiou, G., Maddox, S.J. 1992, ApJ, 390, 338.
- Maker, S., Kurtz, M.J. and La Sala, J. 1982, *The REDUCE/INTERACT Data Reduction System* (Hanover: Dartmouth College Department of Physics and Astronomy).
- Marzke, R.O., Huchra, J.P., Geller, M.J. 1994, ApJ, 428, 43.
- Marzke, R.O., Geller, M.J., Huchra, J.P. and Corwin, H.G. 1994 *AJ*, **108**, 437.
- Marzke, R.O., da Costa, L.N., Pellegrini, P.S. & Willmer, C.N.A. 1997, ApJ, submitted.
- Mohr, J.J., Geller, M.J., Fabricant, D.G., Wegner, G., Thorstensen, J.R. and Richstone, D.O. 1996, ApJ, 470, 724.
- Postman, M., Geller, M.J., and Huchra, J.P. 1988, AJ, 95, 571.
- Ramella, M., Nonino, M. and Geller, M.J. 1995, *Mem.S.A.I.*, 66, 113.
- Rocca-Volmerange, B. & Guiderdoni, B. 1988, A&AS, 75, 93.
- Sandage, A., Tammann, G.A., and Yahil, A. 1979, ApJ, 232, 352.
- Shectman, S.A., Landy, S.D., Oemler, A., Tucker, D.L., Lin, H., Kirshner, R.P., Schechter, P.L. 1996, ApJ, 470, 172
- Schechter, P. 1976, ApJ, 203, 297.
- Small, T., Sargent, W.L.W. and Hamilton, D. 1997, ApJS, 111.1.

- Thorstensen, J.R., Wegner, G.A., Hamwey, R., Boley, F., Geller, M.J., Huchra, J.P., Kurtz, M.J. and Mc Mahan, R.K. 1989, AJ, 98, 1143.
- Thorstensen, J.R., Kurtz, M.J., Geller, M.J., Ringwald, F.A., and Wegner, G. 1995, AJ, 109, 2368.
- Tonry, J. and Davis, M. 1979, AJ, 43, 393.
- Vettolani, G., Zucca, E., Zamorani, G., Cappi, A., Merighi, R., Mignoli, M., Stirpe, G.M., MacGillivray, H., Collins, C., Balkowski, C., Cayette, V., Maurogordato, S., Proust, D., Chincarini, G., Guzzo, L., Maccagni, D., Scaramella, R., Blanchard, A., and Ramella, M., 1997, A&A, in press.
- Willmer, C.N.A., Koo, D.C., Ellman, N., Kurtz, M.J., Szalay and A.S. 1996, ApJS, 104, 199.
- Yahil, A., Strauss, M.A., Davis, M., and Huchra, J.P. 1991, ApJ, 372, 380.
- Zucca, E., Zamorani, G., Vettolani, P., Cappi, A., Merighi, M., Stirpe, G.M., MacGillivray, H., Collins, C., Balkowski, C., Cayette, V., Maurogordato, S., Proust, D., Chincarini, G., Guzzi, L., Maccagni, D., Scaramella, R., Blanchard, A., and Ramella, M. 1997, A&A, submitted.